Complex orientation dependence of Casimir-Polder interaction induced by curvature and optical properties of the surface and the surrounding medium

Giuseppe Bimonte

Dipartimento di Scienze Fisiche, Università di Napoli Federico II, Complesso Universitario di Monte S. Angelo, Via Cintia, I-80126 Napoli, Italy and INFN Sezione di Napoli, I-80126 Napoli, Italy

Thorsten Emig

Laboratoire de Physique Théorique et Modèles Statistiques, CNRS UMR 8626, Université Paris-Saclay, 91405 Orsay cedex, France (Dated: June 26, 2025)

We employ a multiple scattering expansion to systematically derive curvature corrections to the Casimir-Polder (CP) interaction between small an-isotropic particles and general magneto-dielectric surfaces. Our results, validated against exact solutions, reveal a complex, distance-dependent interplay between material properties and surface curvature in determining stable particle orientations. We demonstrate that even small surface curvature can induce or eliminate switches in the preferred orientation, a quantum effect that is diminished by thermal fluctuations. This work provides a crucial understanding of how to engineer nano-particle orientation through tune-able parameters, offering significant implications for micro- and nano-mechanical device design.

Introduction — Particle-surface interactions play a crucial role in numerous physical, chemical, and biological processes [1, 2, 4–6]. While the underlying mechanisms can vary, many such interactions involve neutral particles influenced by fluctuating electromagnetic fields. Recent experimental investigations have focused on understanding how surface geometry, particularly microstructured surfaces, affects dispersion forces [7–12]. Other notable examples include quantum friction [13], heat transfer between nanoparticles [14], and critical Casimir forces in complex systems [15, 16].

This work delves into the realm of van der Waals and Casimir-Polder (CP) forces, arising from quantum and thermal fluctuations of the electromagnetic field. Traditionally studied for planar surfaces [17], these forces exhibit significant modifications in the presence of curved geometries. The proximity force approximation (PFA) [18], commonly used for short-distance interactions, often fails to capture curvature effects accurately. Furthermore, the non-additive nature of these forces can lead to intriguing phenomena for anisotropic particles [19]. For good conductors, the interaction between spheroids scales with the volumes of their enclosing spheres, rather than their actual volumes [20].

A range of computational methods, including perturbative, scattering, and numerical techniques, can be applied to calculate complex Casimir-Polder forces, each with its own advantages and limitations. Early 20th-century scattering techniques [21, 22] are well-suited for distances significantly larger than the radii of curvature. However, their practical applicability is limited to highly symmetric bodies, such as spheres [6, 7] and cylinders [25, 26], or a few perfectly conducting shapes [27]. Additionally, these methods face fundamental limitations in handling interlocked geometries due to the convergence

issues of mode expansions. Within the scattering framework, the Rayleigh expansion has been employed to study atom-nanograting interactions [28]. Perturbative methods [29] are applicable to surfaces with small, smooth corrugations.

An alternative approach that becomes exact in the limit of small particle-surface distances was introduced in [30]. This method involves a systematic expansion of the potential in derivatives of the surface profile, enabling its application to general curved surfaces. A similar technique had been previously employed to study Casimir interactions between non-planar surfaces [31–33], radiative heat transfer [34], and electrostatic forces between conductors [35]. For a recent review of the derivative expansion method, see [36].

Here, we reconsider the problem of the CP potential for an anisotropic particle near a curved surfaces, in the limit where the radii of curvature R_i , j = 1, 2 are much larger than the distance d of the particle from the surface. Thanks to a recently developed surface formulation of a multiple scattering expansion (MSE) for Casimir and Casimir-Polder interactions for magneto-dielectric materials [8, 37, 39, 40], generalizing earlier work by Balian and Duplantier for perfect conductors [41], the CP potential can be computed without any approximation to (at least) first order in d/R_i . At this order, we estimate an error of about 2\% of this expansion for $d/R_i = 0.1$ by comparing to the known potential of a sphere. This result represents a significant advance over earlier work [30]. Firstly, the earlier derivative expansion relied on a reasonable ansatz, justified only a posteriori through a formal re-summation of a perturbative expansion for small in-plane momenta [36]. The MSE provides a simple and direct curvature expansion, without requiring any prior assumptions. Secondly, and practically most important, the earlier approach in [30] is limited to perfect electric conductors (PEC), leaving material effects inaccessible. Combined material and curvature effects turn out be important for the orientation dependence of the CP potential for particles with anisotropic polarizability. We assume that the particle has rotational symmetry about one axis (3-axis) so that the polarizability tensor is diagonal with $\tilde{\alpha}=\mathrm{diag}(\tilde{\alpha}_{\perp}/2,\tilde{\alpha}_{\perp}/2,\tilde{\alpha}_3)$ relative to the principal axes attached to the particle. To linear order in d/R_j , we find for the orientation dependent part of the CP potential at temperature T

$$U_{o}(d,\theta,\phi) = -\frac{k_{B}T}{2d^{3}} \sum_{n=0}^{\infty} ' \sigma(i\xi_{n}) \left[\left\{ \Delta \beta^{(0)}(\bar{\kappa}_{n}) + \Delta \beta^{(2)}(\bar{\kappa}_{n}) \left(\frac{d}{R_{1}} + \frac{d}{R_{2}} \right) \right\} \cos(2\theta) + \beta_{3}^{(2)}(\bar{\kappa}_{n}) \left(\frac{d}{R_{1}} - \frac{d}{R_{2}} \right) \cos(2\phi) \sin^{2}\theta \right]$$
(1)

where $\xi_n = 2\pi k_B T n/\hbar$ are the Matsubara frequencies, $\bar{\kappa}_n = \kappa_n d$ with $\kappa_n = \xi_n/c$, $\sigma = \tilde{\alpha}_3 - \tilde{\alpha}_{\perp}/2$ measures the anisotropy of the particle's (frequency dependent) polarizability, the prime in the sum indicates that the n=0 term is taken with weight one-half, and we define $\Delta \beta^{(0)} = \beta_2^{(0)} - \beta_1^{(0)}$ and $\Delta \beta^{(2)} = \beta_2^{(2)} - \beta_1^{(2)}$, where $\beta_q^{(p)}$ are the coefficients specified in Eq. (4) below. The angle θ is formed by the particle's 3-axis and the z-axis, and ϕ is the polar angle of the 3-axis projected onto the xy-plane. The xyz coordinate system has its origin at P, the point on the surface nearest the particle. The x and y axes align with the principal tangential directions of minimal and maximal surface curvature at P. and the \hat{z} axis is the surface normal oriented from the surface toward the particle. The dimensionless functions $\Delta\beta^{(0)}, \, \Delta\beta^{(2)}, \, \beta_3^{(2)}$ depend on the electric and magnetic permittivities of the surface $(\epsilon_1(i\xi_n), \mu_1(i\xi_n))$ and the embedding medium $(\epsilon_0(i\xi_n), \mu_0(i\xi_n))$. These functions can be evaluated exactly as integrals over the modulus of the in-plane wave vector of analytically known functions but their general form is rather unwieldy, and we provide them in the SI. Note that Eq. (1) requires no assumption about the distance d relative to all material and medium related length scales. If $R_1 \neq R_2$ and the sum of $\beta_3^{(2)}(\bar{\kappa}_n) \neq 0$ it is easy to verify that the potential U_o has a unique minimum which corresponds to an orientation of the particle along one of the three principal directions of the surface (x, y, z). For $R_1 = R_2$ or the sum of $\beta_3^{(2)}(\bar{\kappa}_n)=0$ the particle is oriented either along the z-axis or along any direction in the xy (tangential) plane.

It is known that for a PEC flat surface there is no

orientation dependence of the CP potential at zero temperature for dipolar particles with frequency independent polarizabilities. This can be seen from Eq. (1) since for T=0 the sum is replaced by an integral and $\int_0^\infty d\kappa \, \Delta \beta^{(0)}(\kappa) = 0$. For general surface materials, frequency dependent polarizabilities, or finite temperature, however, the term proportional to $\Delta \beta^{(0)}$ is non-zero in general. Hence in the stable orientation the symmetry axis of the particle is either oriented perpendicular to the surface or can rotate freely in the surface plane. For all studied materials, we find that the preferred orientation does not depend on the distance d of the particle from the surface if the surface is placed in vacuum. But interestingly, as we show here, the preferred orientation can depend on d, if the medium in which the surface is placed has suitable optical properties.

For a *curved* surface the orientation dependence becomes more complex. Remarkably, we find that small surface curvature can induce or eliminate switches in stable particle orientation, with the switching distance depending on material properties and magnitude of curvature. These switches are a quantum effect which is gradually washed out by thermal fluctuations, leading to a distance independent stable orientation in the classical high temperature limit for all considered materials.

Method — The CP potential can be expressed in terms of the 3×3 electric scattering Green tensor $\mathbb{F}^{(EE)}$ [8],

$$U = -4\pi k_B T \sum_{n=0}^{\infty} \kappa_n \sum_{i,j=1}^{3} \alpha_{ij} (i \, \xi_n) \mathbb{F}_{ij}^{(EE)} (\mathbf{r}_0, \mathbf{r}_0; \kappa_n),$$
(2)

where

$$\mathbb{\Gamma}^{(EE)}(\mathbf{r}_0, \mathbf{r}_0; \kappa_n) = \int_S ds_{\mathbf{u}} \int_S ds_{\mathbf{u}'} \sum_{p,q \in \{E,H\}} \mathbb{G}_0^{(Ep)}(\mathbf{r}_0, \mathbf{u}) \left[(\mathbb{I} - \mathbb{K})^{-1} \right]^{(pq)} (\mathbf{u}, \mathbf{u}') \mathbb{M}^{(qE)}(\mathbf{u}', \mathbf{r}_0)$$
(3)

can be expressed in terms of surface operators \mathbb{K} , \mathbb{M} which are integrated over the surface S. These opera-

tors can be expressed in terms of the free Green tensor \mathbb{G}_0 and \mathbb{G}_1 for homogeneous space with permittivities

 ϵ_0 , μ_0 and ϵ_1 , μ_1 , respectively, see SI. We parametrize the surface S as $\mathbf{s}(u_1,u_2)=u_1\hat{\mathbf{x}}+u_2\hat{\mathbf{y}}+h(u_1,u_2)\hat{\mathbf{z}}=u_1\hat{\mathbf{x}}+u_2\hat{\mathbf{y}}+\frac{1}{2}h_{\alpha\beta}u_{\alpha}u_{\beta}\hat{\mathbf{z}}+\dots$ where repeated indices are summed over and the height profile h and its first derivatives vanish at the point $(u_1,u_2)=(0,0)$, corresponding to the closest surface position to the particle. Here $h_{\alpha\beta}=\partial^2 h/\partial_{u_\alpha}\partial_{u_\beta}(0,0)$ denotes the second derivatives at that position. The outward surface normal vector $\mathbf{n}=\tilde{\mathbf{n}}/\sqrt{1+(\partial h/\partial_{u_1})^2+(\partial h/\partial_{u_2})^2}$ to lowest order in curvature is given by $\tilde{\mathbf{n}}=\hat{\mathbf{z}}-\hat{\mathbf{x}}h_{1\alpha}u_{\alpha}-\hat{\mathbf{y}}h_{2\alpha}u_{\alpha}$ We note that the normalizing square root can be ignored when evaluating Eq. (3) as it cancels against the surface element from the surface integrals. To lowest order in curvature, all operators in Eq. (3) depend only on the second derivatives $h_{\alpha\beta}$. We use the Fourier representa-

tion of the free Green tensors \mathbb{G}_0 and \mathbb{G}_1 and expand all operators to linear order in $h_{\alpha\beta}$. The integrations over the wave vector along the $\hat{\mathbf{z}}$ direction and the angle of the in-plane $\hat{\mathbf{x}}$ - $\hat{\mathbf{y}}$ wave vector can be carried out analytically, yielding for $\mathbb{F}^{(EE)}$ a curvature expansion which depends only on $\bar{\kappa}_n$, the modulus k of the in-plane wave vector and the permittivities, see SI. The k-integrals of the coefficients in this curvature expansion define coefficients $\beta_l^{(m)}$ with m=0 for a flat surface $(h_{\alpha\beta}=0)$ and m=2 for the first order curvature corrections $\sim h_{\alpha\beta}$.

When the components of the polarizability tensor are expressed relative to the principal directions of surface curvature at the point of the surface which is closest to the particle, the CP potential at temperature T reads

$$U = -\frac{k_B T}{d^3} \sum_{n=0}^{\infty} \left\{ \beta_1^{(0)} \alpha_{\perp} + \beta_2^{(0)} \alpha_{zz} + d \left[(\beta_1^{(2)} \alpha_{\perp} + \beta_2^{(2)} \alpha_{zz}) \nabla^2 h + \beta_3^{(2)} \left(\partial_i \partial_j h - \frac{1}{2} \nabla^2 h \delta_{ij} \right) \alpha_{ij} \right] \right\} , \tag{4}$$

where α is the particles' electric dipole polarizability in the xyz coordinate system, $\alpha_{\perp} = \alpha_{xx} + \alpha_{yy}$, and α_{ij} can depend on ξ_n while the functions $\beta_q^{(p)}$ depend on $\bar{\kappa}_n$. In the limit $T \to 0$, the summation is replaced by an integration according to $k_B T \sum_{n=0}^{'\infty} \to \frac{\hbar c}{d} \int_0^\infty \frac{d\bar{\kappa}}{2\pi}$. Note that the same expression for U applies to particles with magnetic polarizability but with different functions $\beta_q^{(p)}$. A geometrical interpretation of Eq. (4) becomes apparent with the local expansion $h = x^2/(2R_1) + y^2/(2R_2) + \dots$ around the point of the surface which is closest to the particle, where R_1 and R_2 are the radii of curvature. Below, we consider the materials Gold (Au), Silicon (Si) and Polystyrene (PS). The medium outside the surface is either vacuum (V) or Bromobenzene (Br). The dielectric functions of these materials are provided in the SI.

Validity range of curvature expansion — The validity range of the small curvature expansion of Eq. (4) can be estimated as the exact CP potential for the special case of a spherical surface is known from a scattering approach [7]. For simplicity, here we consider a particle with isotropic, frequency independent polarizability $\alpha_{ij} = \alpha \, \delta_{ij}$ at distance d from a dielectric sphere of radius R in vacuum ($\epsilon_0 = \mu_0 = 1$). The scattering approach yields for the CP potential a sum over partial waves of a lengthy expression of combinations of Bessel functions, see SI. Fig. (1) in the SI displays the ratios of the approximate CP potential U_k (truncated at the k-th power of d/R) to the exact potential $U_{\rm sphere}$ for a Au sphere with a radius of $R = 30 \mu \text{m}$ at T = 300 K, as a function of the ratio d/R. The curvature expansion is remarkably accurate: For the smallest considered d/R value of 0.07, the flat surface approximation U_0 yields a relative error of 7.6%. When the leading curvature correction is

included, for U_1 the error reduces to 0.5%.

Stable orientations — Now we demonstrate how surface curvature affects stable particle orientations, using Eq. (1). We consider two different types of particles: (1) a generic particle with a frequency independent polarization anisotropy σ , and (2) an ellipsoidal particle made of gold, silicon or polystyrene, where the now frequency dependent polarization anisotropy is given by [42]

$$\sigma(i\xi) = \frac{\epsilon_0(\epsilon_1 - \epsilon_0)^2 (1 - 3n_z) V}{[\epsilon_0(1 - n_z) + \epsilon_1 n_z] [\epsilon_0(1 + n_z) + \epsilon_1 (1 - n_z)]}, (5)$$

where $\epsilon_1 \equiv \epsilon_1(\mathrm{i}\,\xi), \; \epsilon_0 \equiv \epsilon_0(\mathrm{i}\,\xi), \; V$ is the particle's volume and n_z is the depolarization factor which is given by the eccentricity of the particle. For a disk-like particle $1/3 < n_z < 1$, and for a needle-like particle $0 < n_z < 1/3$. From Eq. (5), it is apparent that $\sigma < 0$ for a disk-like particle, whereas $\sigma > 0$ for a needle-like particle. The surface is made of the same material as the particle. The surrounding medium is either vacuum or Bromobenzene. With $\sigma(i\xi)$ substituted in Eq. (1) we determine the particle orientation with minimal $U_o(d, \theta, \phi)$. For T = 0 K the stable axes as function of the surface-particle distance d(between 100nm and $10\mu m$) and the distance to curvature ratios are shown for Au in vacuum in Fig. 1, for Au in Br in Fig. 2 and for polystyrene in Br in Fig. 3. Here positive (negative) radii of curvature mean that the surface is curved towards (away from) the particle. Shown is only the region with $d/R_1 \ge d/R_2$ since the stability diagrams for $d/R_1 \leq d/R_2$ is obtained by the replacement $z \to z$, $x \to y, y \to x$ for the stable axis. For Au in vacuum the symmetry axis of a disk-like particle is oriented typically along the x-axis but there exists a small region where the particle orients along the z axis above a curvature dependent distance d. A needle-like particle is oriented along the z-axis in proximity to the surface and aligned with the y-axis for larger distances. The switching distance depends (weakly) on the particle eccentricity via n_z . For Au in Br, the stability diagram is more complex. For a flat surface there can be two switches of stable orientation with distance for both disk- and needle-like particles. One or both of these switches can be eliminated due to surface curvature, depending on the relative magnitude of distance and radii of curvature. For polystyrene in vacuum a disk-like (needle-like) particle is always oriented along the x- or y-axis (z-axis), independent of distance and curvature. However, for polystyrene in Br, only a

disk-like particle's orientation along the z-axis is independent of distance and curvature. A needle-like particle switches orientation at a curvature independent distance between x-axis close to the surface and y-axis at larger surface separation. The switching distance depends on the eccentricity of the particle. Finally, for Si in either vacuum or Br, a needle-like (disk-lie particle) is always oriented along the z-axis (x- or y-axis), and hence no stability plot is shown for this case.

Next, we consider the effect of thermal fluctuations. It is instructive to consider first the high temperature limit corresponding to the n=0 term in Eq. (4) only. The orientation dependent CP potential becomes in this limit

$$U_o = -\frac{k_B T \sigma}{32 \epsilon_0 d^3} \left[\left\{ \frac{\epsilon_1 - \epsilon_0}{\epsilon_1 + \epsilon_0} - \frac{(\epsilon_1 - \epsilon_0)^2}{4(\epsilon_1 + \epsilon_0)^2} \left(\frac{d}{R_1} + \frac{d}{R_2} \right) \right\} \cos(2\theta) + \frac{(\epsilon_1 - \epsilon_0)(3\epsilon_1 + \epsilon_0)}{4(\epsilon_1 + \epsilon_0)^2} \left(\frac{d}{R_1} - \frac{d}{R_2} \right) \cos(2\phi) \sin^2 \theta \right]$$
(6)

where σ and the permittivities are the static values here. Note that the potential is independent of the magnetic permittivities due to the decoupling of electric and magnetic modes in the static limit. From this result we find that for Au in vacuum or in Br, for Si in vacuum or in Br, and for polystyrene in vacuum a needle-like particle is always oriented along the z-axis and a disklike particle along the x-axis (y-axis) for $1/R_1 > 1/R_2$ $(1/R_1 < 1/R_2)$. However, for polystyrene in Br the stable orientation is the opposite: along the z-axis for a disklike particle and along the x- or y-axis for a needle-like particle. This shows that thermal fluctuations remove the switches of stable orientation with distance. At room temperature (T = 300K), the stable orientations are the same as in the high temperature limit with the exception of Au in Br. For this case the stability diagram in shown in Fig. 4. Compared to the high temperature limit, regions with switched stable orientation proliferate at intermediate distances, and their size depends both on the magnitude of surface curvature and the eccentricity of the particle.

Discussion — In this work, we have employed a MSE to derive curvature corrections to the CP interaction between small anisotropic particles and general magneto-dielectric surfaces. This approach represents a significant advancement over earlier derivative expansion methods, particularly in its ability to handle material effects and provide a direct curvature expansion without prior assumptions. We have derived an orientation-dependent CP potential, valid to linear order in d/R_j , where d is the particle-surface distance and R_j are the radii of curvature. Our results reveal complex and intriguing phenomena concerning the stable orientations of anisotropic nano-particles near curved surfaces. We show that the

preferred particle orientation can depend on the distance d from the surface, especially when the surrounding medium possesses specific optical properties. Crucially, we find that even small surface curvatures can induce or eliminate switches in stable particle orientation. These orientation switches are identified as a quantum effect, which diminishes with increasing thermal fluctuations, leading to a distance-independent stable orientation in the classical high-temperature limit. We illustrated these effects for various material combinations, including Gold, Silicon, and Polystyrene surfaces in vacuum or Bromobenzene. Our findings demonstrate that a strategic combination of material properties, surface curvature, and temperature can be effectively utilized to engineer and control the orientation of nano-particles in the vicinity of surfaces. This comprehensive theoretical framework provides valuable insights for the design and optimization of micro- and nano-mechanical devices leveraging these fundamental interactions.

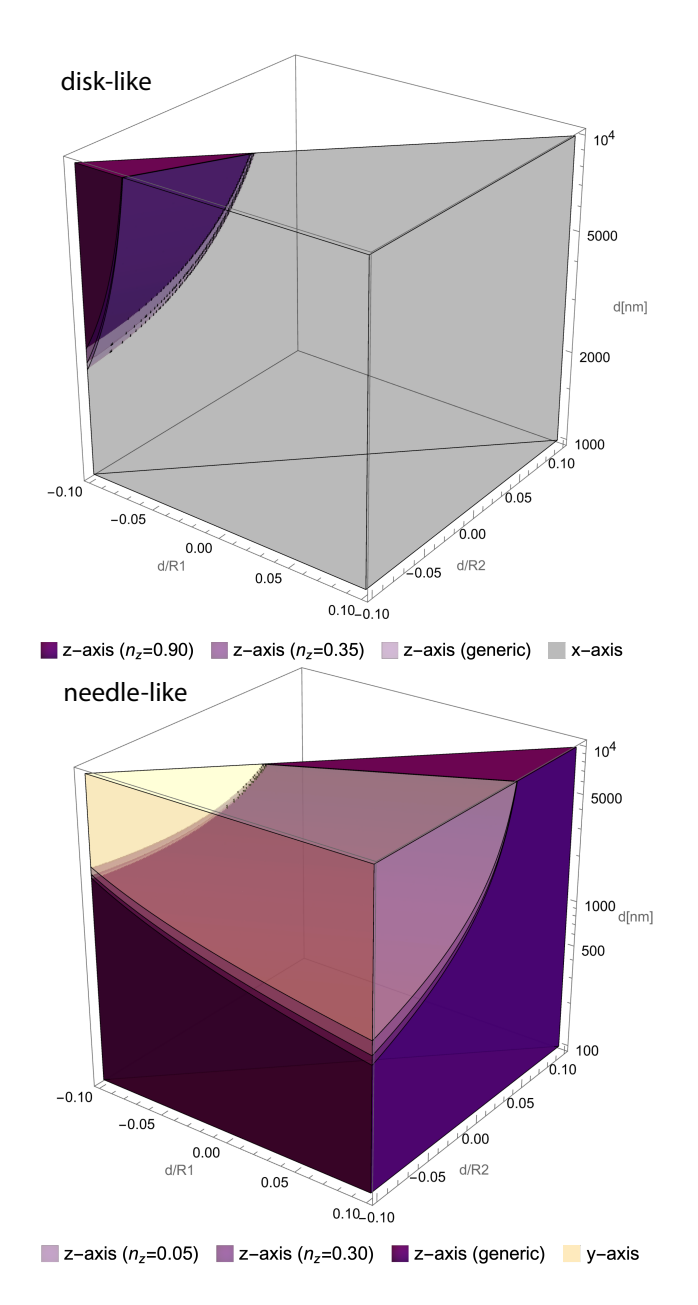
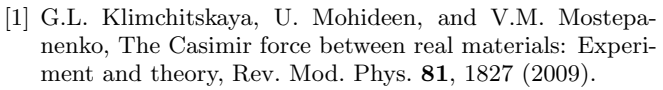


FIG. 1. Stability diagram for Au surface in vacuum at T=0 K: For a flat surface $(d/R_1=d/R_2=0)$ a disk-like (needle-like) particle positions itself with the symmetry axis parallel (perpendicular) to the surface at all distances d. For a curved surface, the stable direction can change with distance, depending on the radii of surface curvature.



^[2] Casimir Physics, edited by D.A.R. Dalvit et al., Lecture Notes in Physics Vol. 834 (Springer, New York, 2011).

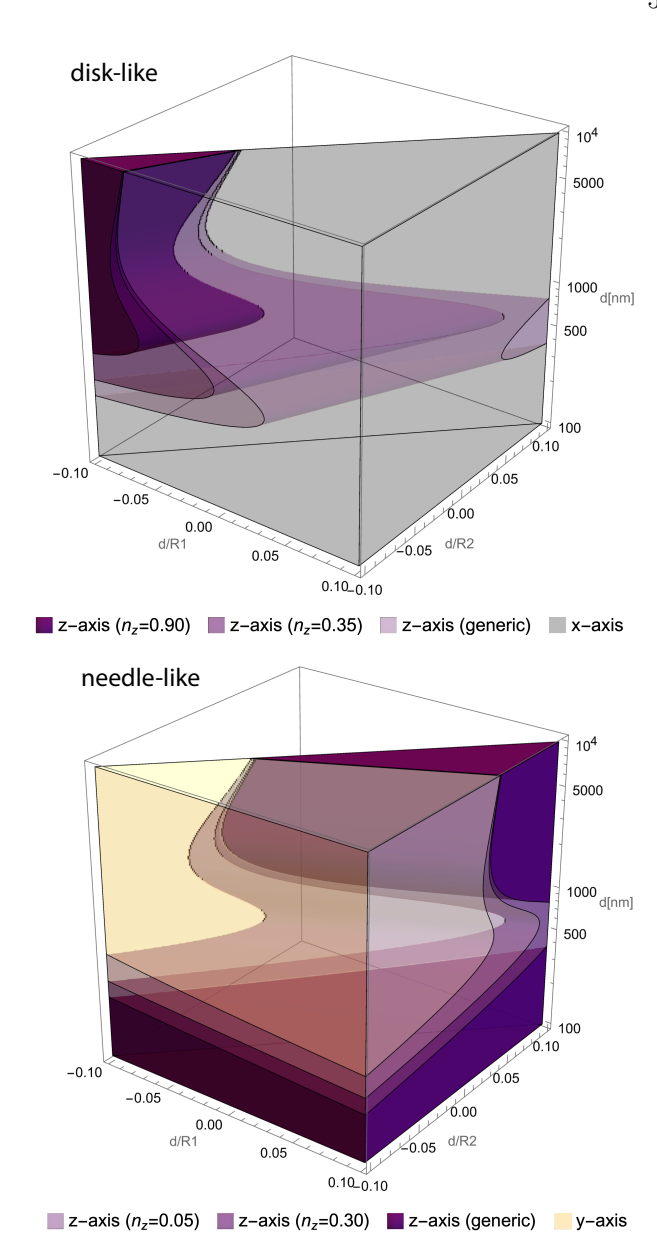


FIG. 2. Stability diagram for Au surface in Br at $T=0~\rm K$: For a flat surface $(d/R_1=d/R_2=0)$ the preferred orientation can change twice with distance, depending on the details of the particle's polarizability: A disk-like (needle-like) particle tends to position itself with the symmetry axis perpendicular (parallel) to the surface at intermediate distances d. For a curved surface, the one or both orientation switches can be eliminated, depending on curvature magnitude.

- [4] S.Y. Buhmann, Dispersion Forces. I: Macroscopic Quantum Electrodynamics and Ground-State Casimir, Casimir Polder, and van der Waals Forces (Springer: Berlin/Heidelberg, Germany, 2012).
- [5] L. M. Woods, D.A.R. Dalvit, A. Tkatchenko, P. Rodriguez-Lopez, A.W.Rodriguez and R. Podgornik, Materials perspective on Casimir and van der Waals interactions, Rev. Mod. Phys. 88, 045003 (2016).
- [6] G. Bimonte, T. Emig, M. Kardar, and M. Krüger, Nonequilibrium Fluctuational Quantum Electrodynamics:

^[3] V. A. Parsegian, Van der Waals Forces: A Handbook for Biologists, Chemists, Engineers, and Physicists (Cambridge University Press: New York, NY, USA, 2006).

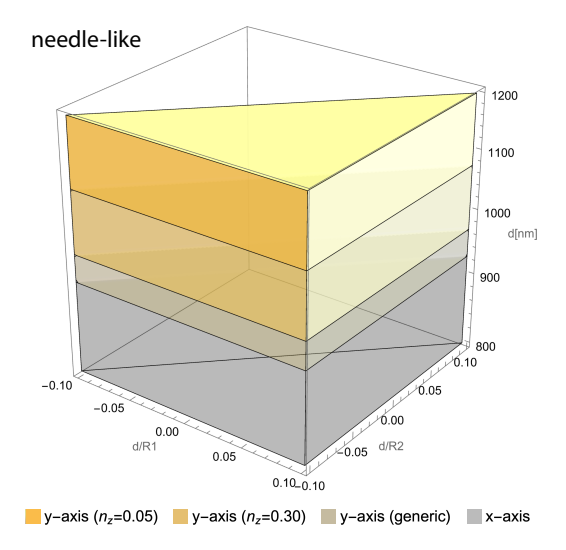
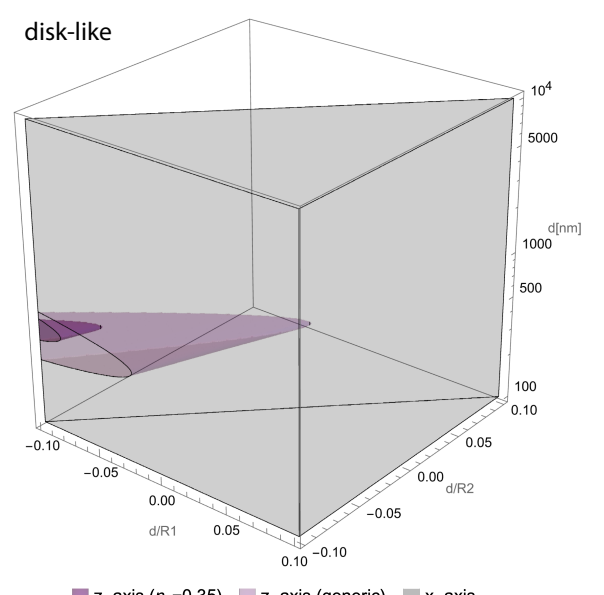


FIG. 3. Stability diagram for polystyrene surface in Br at T=0 K: For both a flat surface $(d/R_1=d/R_2=0)$ and a curved surface, a needle-like particle positions itself with the symmetry axis parallel to the surface but the preferred tangential direction depends on distance. A disk-like particle positions itself with the symmetry axis perpendicular to the surface at all distances.

Heat Radiation, Heat Transfer, and Force, Annu. Rev. Condens. Matter Phys. 8, 119 (2017).

- [7] T. A. Pasquini, M. Saba, G.-B. Jo, Y. Shin, W. Ketterle, D. E. Pritchard, T. A. Savas, and N. Mulders, Low velocity quantum reflection of Bose-Einstein condensates, Phys. Rev. Lett. 97, 093201 (2006).
- [8] H. Oberst, D. Kouznetsov, K. Shimizu, J. I. Fujita, and F. Shimizu, Fresnel diffraction mirror for an atomic wave, Phys. Rev. Lett. 94, 013203 (2005).
- [9] B. S. Zhao, S. A. Schulz, S. A. Meek, G. Meijer, and W. Schollkopf, Quantum reflection of helium atom beams from a microstructured grating, Phys. Rev. A 78, 010902(R) (2008).
- [10] J. D. Perreault, A. D. Cronin, and T. A. Savas, Using atomic diffraction of Na from material gratings to measure atom-surface interactions, Phys. Rev. A 71, 053612 (2005).
- [11] V. P. A. Lonij, W. F. Holmgren, and A. D. Cronin, Magic ratio of window width to grating period for van der Waals potential measurements using material gratings, Phys. Rev. A 80, 062904 (2009).
- [12] H. Bender, C. Stehle, C. Zimmermann, S. Slama, J. Fiedler, S. Scheel, S. Y. Buhmann, and V. N. Marachevsky, Probing Atom-Surface Interactions by Diffraction of Bose-Einstein Condensates, Phys. Rev. X 4, 011029 (2014).
- [13] J. B. Pendry, Shearing the vacuum quantum friction, J. Phys.: Condens. Matter 9, 10301 (1997).
- [14] S. A. Biehs and J. J. Greffet, Near-field heat transfer between a nanoparticle and a rough surface, Phys. Rev. B 81, 245414 (2010).
- [15] O. A. Vasilyev, E. Eisenriegler, and S. Dietrich, Critical Casimir torques and forces acting on needles in two spatial dimensions, Phys. Rev. E 88, 012137 (2013).
- [16] S. Kondrat, L. Harnau, and S. Dietrich, Critical Casimir



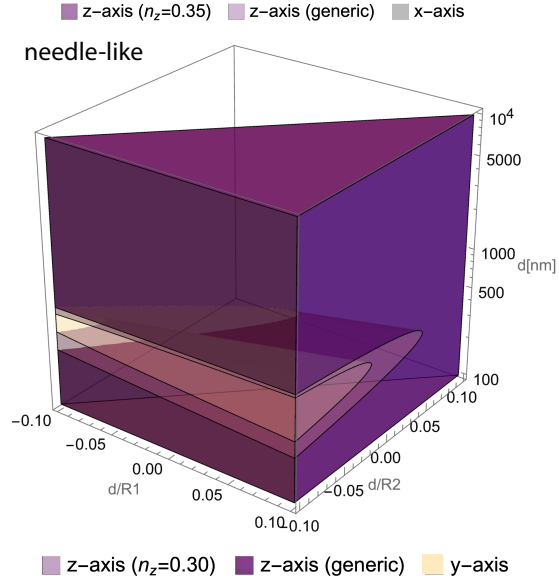


FIG. 4. Stability diagram for Au surface in Br at $T=300~\rm K$: Compared to zero temperature, the generic stability regions (x-axis for a disk-like particle, z-axis for a needle-like particle) are enlarged by thermal fluctuations. However, two changes of preferred orientation are still possible, depending on the curvature magnitude.

interaction of ellipsoidal colloids with a planar wall, J. Chem. Phys. ${\bf 131},\,204902$ (2009).

- [17] H.B.G. Casimir and D. Polder, The Influence of retardation on the London-van der Waals forces, Phys. Rev. 73, 360 (1948).
- [18] B. V. Derjaguin and I.I. Abrikosova, Direct measurement of the molecular attraction of solid bodies. 1. Statement of the problem and method of measuring forces by using negative feedback, Sov. Phys. JETP 3, 819 (1957); B. V. Derjaguin, The Force Between Molecules, Sci. Am. 203, 47 (1960).
- [19] K. A. Milton, E. K. Abalo, P. Parashar, et al., Three-

- body effects in Casimir-Polder repulsion, Phys. Rev. A 91, 042510 (2015).
- [20] T. Emig, N. Graham, R. L. Jaffe, and M. Kardar, Orientation dependence of Casimir forces, Phys. Rev. A 79, 054901 (2009).
- [21] A. Lambrecht, P. A. Maia Neto, and S. Reynaud, The Casimir effect within scattering theory, New J. Phys. 8, 243 (2006).
- [22] T. Emig, N. Graham, R. L. Jaffe, and M. Kardar, Casimir forces for arbitrary compact objects, Phys. Rev. Lett. 99, 170403 (2007).
- [23] V. N. Marachevsky, Casimir Effect and Quantum Field Theory in dielectrics, Theor. Math. Phys. 131, 468 (2002).
- [24] S.Y. Buhmann H.T. Dung, D.G. Welsch, The van der Waals energy of atomic systems near absorbing and dispersing bodies, J. Opt. B Quantum Semiclass. Opt. 6, S127 (2004).
- [25] V.B. Bezerra, E.R. Bezerra de Mello, G.L. Klimchitskaya, V.M. Mostepanenko, and A.A. Saharian, Exact Casimir-Polder potential between a particle and an ideal metal cylindrical shell and the proximity force approximation, Eur. Phys. J. C 71, 1614 (2011).
- [26] K.A. Milton, P. Parashar and N. Pourtolami, Casimir-Polder repulsion: Polarizable atoms, cylinders, spheres, and ellipsoids, Phys. Rev. D 85, 025008 (2012).
- [27] M.F. Maghrebi, S.J. Rahi, T. Emig, N. Graham, R.L. Jaffe and M. Kardar, Analytical results on Casimir forces for conductors with edges and tips, Proc. Natl. Acad. Sci. USA 108, 6867 (2011).
- [28] S. Y. Buhmann, V. N. Marachevsky, and S. Scheel, Impact of anisotropy on the interaction of an atom with a one-dimensional nano-grating, Int. J. Mod. Phys. A 31, 1641029 (2016).
- [29] R. Messina, D.A.R. Dalvit, P. A. Maia Neto, A. Lambrecht, and S. Reynaud, Dispersive interactions between atoms and nonplanar surfaces, Phys. Rev. A 80, 022119 (2009).
- [30] G. Bimonte, T. Emig, and M. Kardar, Casimir-Polder force between anisotropic nanoparticles and gently curved surfaces, Phys. Rev. D 92, 025028 (2015).
- [31] C. D. Fosco, F. C. Lombardo, and F. D. Mazzitelli, Proximity force approximation for the Casimir energy as a derivative expansion, Phys. Rev.D 84, 105031 (2011).
- [32] G. Bimonte, T. Emig, R. L. Jaffe, and M. Kardar, Casimir forces beyond the proximity approximation, EPL 97, 50001 (2012).
- [33] G. Bimonte, T. Emig, and M. Kardar, Material dependence of Casimir forces: Gradient expansion beyond proximity, Appl. Phys. Lett. 100, 074110 (2012).
- [34] V.A. Golyk, M. Krüger, A.P. McCauley, and M. Kardar, Small distance expansion for radiative heat transfer between curved objects, EPL 101, 34002 (2013).
- [35] C. D. Fosco, F. C. Lombardo, and F. D. Mazzitelli, Electrostatic interaction due to patch potentials on smooth conducting surfaces, Phys. Rev. A 88, 062501 (2013).
- [36] C. D. Fosco, F. C. Lombardo, and F. D. Mazzitelli, Casimir Physics beyond the Proximity Force Approximation: The Derivative Expansion, Physics **6**, 290 (2024).
- [37] T. Emig and G. Bimonte, Multiple scattering expansion for dielectric media: Casimir effect, Phys. Rev. Lett. 130, 200401 (2023).
- [38] G. Bimonte and T. Emig, Casimir and Casimir-Polder interactions for magneto-dielectric materials: Surface scattering expansion, Phys. Rev. A 108, 052807 (2023).

- [39] G. Bimonte and T. Emig, Surface scattering expansion of the Casimir-Polder interaction for magneto-dielectric bodies: convergence properties for insulators, conductors, and semiconductors, Physics 6, 194 (2024).
- [40] T. Emig, Surface scattering expansion for the Casimir-Polder interaction of a dielectric wedge, Phys. Rev. A 110, 062809 (2024).
- [41] R. Balian and B. Duplantier, Electromagnetic waves near perfect conductors. I. Multiple scattering expansions. Distribution of modes, Ann. Phys. 104, 300 (1977); Electromagnetic waves near perfect conductors. II. Casimir effect, Ann. Phys. 112, 165 (1978).
- [42] A. Sihvola, Electromagnetic mixing formulas and applications (The Institution of Engineering and Technology, London, U.K. 2008).

SUPPLEMENTARY INFORMATION

Parameters of the dielectric functions

In our computations we used for the permittivities of the materials the expressions

$$\epsilon_{\text{Au}}(i\,\xi) = 1 + \frac{\Omega_p^2}{\xi(\xi+\gamma)} + \sum_i \frac{f_j}{\omega_j^2 + g_j\xi + \xi^2},$$
(7)

$$\epsilon_{\rm Si}(i\,\xi) = \epsilon_{\infty}^{\rm (Si)} + \frac{\epsilon_0^{\rm (Si)} - \epsilon_{\infty}^{\rm (Si)}}{1 + \xi^2/\omega_{\rm UV}^2} \,, \tag{8}$$

$$\epsilon_{\text{polystyrene}}(i\,\xi) = 1 + \sum_{j} \frac{f_j}{\omega_j^2 + g_j \xi + \xi^2} \,,$$
 (9)

$$\epsilon_{\text{bromobenzene}}(i\,\xi) = 1 + \frac{C_{\text{IR}}}{1 + \xi^2/\tilde{\omega}_{\text{IR}}^2} + \frac{C_{\text{UV}}}{1 + \xi^2/\tilde{\omega}_{\text{UV}}^2} , \qquad (10)$$

where $\Omega_p = 9 \text{ eV}/\hbar$, $\gamma = 0.035 \text{ eV}/\hbar$ [1], $\epsilon_{\infty}^{(\text{Si})} = 1.035$, $\epsilon_0^{(\text{Si})} = 11.87$, $\omega_{\text{UV}} = 4.34 \text{ eV}/\hbar$, $C_{\text{IR}} = 2.967$, $C_{\text{UV}} = 1.335$, $\tilde{\omega}_{\text{IR}} = 0.360 \text{ eV}/\hbar$, $\tilde{\omega}_{\text{UV}} = 8.465 \text{ eV}/\hbar$ [2, 3], and the oscillator parameters ω_j , f_j , g_j for Au and polystyrene are listed in Tables (I) and (II) respectively.

$\omega_j \; (\mathrm{eV}/\hbar)$	$f_j \; (\mathrm{eV}^2/\hbar^2)$	$g_j \; (\mathrm{eV}/\hbar)$
3.05	7.091	0.75
4.15	41.46	1.85
5.4	2.7	1.0
8.5	154.7	7.0
13.5	44.55	6.0
21.5	309.6	9.0

TABLE I. Oscillator parameteres for Au [4]

$\overline{\omega_j \ (\mathrm{eV}/\hbar)}$	$f_j \; (\mathrm{eV}^2/\hbar^2)$	$g_j \; (\mathrm{eV}/\hbar)$
6.35	14.6	0.65
14.0	96.9	5.0
11.0	44.4	3.5
20.1	136.9	11.5

TABLE II. Oscillator parameteres for polystyrene [5]

Partial wave scattering for a sphere

In the partial wave scattering approach, the CP potential can be written as [6, 7]

$$U_{\text{sphere}} = \frac{k_B T}{a^2} \sum_{n=0}^{\infty} \kappa_n \alpha(\mathrm{i}\,\xi_n) \sum_{l=1}^{\infty} (2l+1) \left\{ T_l^{\text{HH}}(\mathrm{i}\,\xi_n) \mathcal{K}_l^2(\kappa_n a) - T_l^{\text{EE}}(\mathrm{i}\,\xi_n) \left[\mathcal{K}_l^{'2}(\kappa_n a) + \frac{l(l+1)}{\kappa_n^2 a^2} \mathcal{K}_l^2(\kappa_n a) \right] \right\} ,$$

where a = R + d, l is the multipole index, $\mathcal{K}'_l(x) = d\mathcal{K}_l/dx$, $\mathcal{K}_l(x) = xk_l(x)$, $k_l(x) = \sqrt{\frac{2}{\pi x}}K_{l+1/2}(x)$ is the modified spherical Bessel function of the third kind, and T_l^{HH} , T_l^{EE} are the T-matrix elements (Mie coefficients) of the sphere,

$$T_l^{\rm HH}(i\xi) = \frac{\sqrt{\mu/\epsilon} \,\mathcal{I}_l(\sqrt{\epsilon\mu}\kappa R) \,\mathcal{I}_l'(\kappa R) - \mathcal{I}_l'(\sqrt{\epsilon\mu}\kappa R) \,\mathcal{I}_l(\kappa R)}{\mathcal{K}_l(\kappa R) \,\mathcal{I}_l'(\sqrt{\epsilon\mu}\kappa R) - \sqrt{\mu/\epsilon} \,\mathcal{I}_l(\sqrt{\epsilon\mu}\kappa R) \,\mathcal{K}_l'(\kappa R)}, \qquad (11)$$

$$T_l^{\text{EE}}(i\xi) = \frac{\sqrt{\epsilon/\mu} \, \mathcal{I}_l(\sqrt{\epsilon\mu\kappa}R) \, \mathcal{I}_l'(\kappa R) - \mathcal{I}_l'(\sqrt{\epsilon\mu\kappa}R) \, \mathcal{I}_l(\kappa R)}{\mathcal{K}_l(\kappa R) \, \mathcal{I}_l'(\sqrt{\mu/\epsilon\kappa}R) - \sqrt{\epsilon/\mu} \, \mathcal{I}_l(\sqrt{\epsilon\mu\kappa}R) \, \mathcal{K}_l'(\kappa R)},$$
(12)

(13)

where $\xi = \kappa c$, $\mathcal{I}_l(x) = xi_l(x)$ and $\mathcal{I}'_l(x) = d\mathcal{I}_l/dx$ with $i_l(x) = \sqrt{\frac{\pi}{2x}}I_{l+1/2}(x)$ the modified spherical Bessel function of the first kind. Fig. (1) displays the ratios of the approximate CP potential U_k (truncated at the k-th power of d/R) to the exact potential $U_{\rm sphere}$ for a Au sphere with a radius of $R = 30\mu m$ at T = 300K, as a function of the ratio d/R. The curvature expansion is remarkably accurate: For the smallest considered d/R value of 0.07, the flat surface approximation U_0 yields a relative error of 7.6%. When the leading curvature correction is included, for U_1 the error reduces to 0.5%.

Derivative expansion within the MSE

Here we provide details on the expansion of the CP potential in surface curvature, based on the MSE presented in Ref. [8]. The components of 6×6 dimensional Green tensor then are

$$\mathbb{G}_{\sigma,ij}^{(EE)}(\mathbf{r},\mathbf{r}') = -\frac{1}{\kappa} \left(\frac{1}{\epsilon_{\sigma}} \frac{\partial^{2}}{\partial x_{i} \partial x'_{j}} + \mu_{\sigma} \kappa^{2} \delta_{ij} \right) g_{\sigma}(\mathbf{r} - \mathbf{r}') ,$$

$$\mathbb{G}_{\sigma,ij}^{(HH)}(\mathbf{r},\mathbf{r}') = -\frac{1}{\kappa} \left(\frac{1}{\mu_{\sigma}} \frac{\partial^{2}}{\partial x_{i} \partial x'_{j}} + \epsilon_{\sigma} \kappa^{2} \delta_{ij} \right) g_{\sigma}(\mathbf{r} - \mathbf{r}') ,$$

$$\mathbb{G}_{\sigma,ij}^{(HE)}(\mathbf{r},\mathbf{r}') = -\epsilon_{ijk} \frac{\partial}{\partial x_{k}} g_{\sigma}(\mathbf{r} - \mathbf{r}') ,$$

$$\mathbb{G}_{\sigma,ij}^{(EH)}(\mathbf{r},\mathbf{r}') = -\epsilon_{ijk} \frac{\partial}{\partial x'_{k}} g_{\sigma}(\mathbf{r} - \mathbf{r}') ,$$
(14)

where $i, j \in \{x, y, z\}$ denote the spatial components, σ labels the Green tensor in the surrounding space ($\sigma = 0$) and the body ($\sigma = 1$), ϵ_{ijk} is the Levi-Civita symbol, and the scalar Green function is

$$g_{\sigma}(\mathbf{r} - \mathbf{r}') = \frac{e^{-\kappa\sqrt{\epsilon_{\sigma}\mu_{\sigma}}|\mathbf{r} - \mathbf{r}'|}}{4\pi |\mathbf{r} - \mathbf{r}'|}.$$
 (15)

The surface operators, defined for positions \mathbf{s} , \mathbf{s}' on the surface, are expressed in terms of the Green tensor as

$$\mathbb{K}^{(EE)}(\mathbf{s}, \mathbf{s}') = \frac{2}{\mu_0 + \mu_1} \mathbf{n}(\mathbf{s}) \times \left[\mu_0 \mathbb{G}_0^{(HE)}(\mathbf{s}, \mathbf{s}') - \mu_1 \mathbb{G}_1^{(HE)}(\mathbf{s}, \mathbf{s}') \right]
\mathbb{K}^{(HH)}(\mathbf{s}, \mathbf{s}') = \frac{2}{\epsilon_0 + \epsilon_1} \mathbf{n}(\mathbf{s}) \times \left[-\epsilon_0 \mathbb{G}_0^{(EH)}(\mathbf{s}, \mathbf{s}') + \epsilon_1 \mathbb{G}_1^{(EH)}(\mathbf{s}, \mathbf{s}') \right]
\mathbb{K}^{(EH)}(\mathbf{s}, \mathbf{s}') = \frac{2}{\mu_0 + \mu_1} \mathbf{n}(\mathbf{s}) \times \left[\mu_0 \mathbb{G}_0^{(HH)}(\mathbf{s}, \mathbf{s}') - \mu_1 \mathbb{G}_1^{(HH)}(\mathbf{s}, \mathbf{s}') \right]
\mathbb{K}^{(HE)}(\mathbf{s}, \mathbf{s}') = \frac{2}{\epsilon_0 + \epsilon_1} \mathbf{n}(\mathbf{s}) \times \left[-\epsilon_0 \mathbb{G}_0^{(EE)}(\mathbf{s}, \mathbf{s}') + \epsilon_1 \mathbb{G}_1^{(EE)}(\mathbf{s}, \mathbf{s}') \right]$$
(16)

and

$$\mathbb{M}^{(EE)}(\mathbf{s}, \mathbf{r}) = \frac{2\mu_0}{\mu_0 + \mu_1} \mathbf{n}(\mathbf{s}) \times \mathbb{G}_0^{(HE)}(\mathbf{s}, \mathbf{r}) ,$$

$$\mathbb{M}^{(EH)}(\mathbf{s}, \mathbf{r}) = \frac{2\mu_0}{\mu_0 + \mu_1} \mathbf{n}(\mathbf{s}) \times \mathbb{G}_0^{(HH)}(\mathbf{s}, \mathbf{r})
\mathbb{M}^{(HE)}(\mathbf{s}, \mathbf{r}) = -\frac{2\epsilon_0}{\epsilon_0 + \epsilon_1} \mathbf{n}(\mathbf{s}) \times \mathbb{G}_0^{(EE)}(\mathbf{s}, \mathbf{r}) ,$$

$$\mathbb{M}^{(HH)}(\mathbf{s}, \mathbf{r}) = -\frac{2\epsilon_0}{\epsilon_0 + \epsilon_1} \mathbf{n}(\mathbf{s}) \times \mathbb{G}_0^{(EH)}(\mathbf{s}, \mathbf{r}) ,$$
(17)

where $\mathbf{n}(\mathbf{s})$ is the outward pointing surface normal vector. We parametrize the surface as

$$\mathbf{s}(u_1, u_2) = u_1 \hat{\mathbf{x}} + u_2 \hat{\mathbf{y}} + h(u_1, u_2) \hat{\mathbf{z}}$$

$$= u_1 \hat{\mathbf{x}} + u_2 \hat{\mathbf{y}} + \frac{1}{2} h_{\alpha\beta} u_{\alpha} u_{\beta} \hat{\mathbf{z}} + \dots$$
(18)

where we expanded the height profile h to second order

and made use of the fact that h and its first derivative vanish at the origin $u_1 = u_2 = 0$ as the directions $\hat{\mathbf{x}}$, $\hat{\mathbf{y}}$ are chosen to be the tangential directions of the surface at the origin. Next we expand all operators to linear

order in $h_{\alpha\beta}$ and denote by $\overset{\circ}{\mathbb{G}}_{\sigma}$, $\overset{\circ}{\mathbb{K}}$ and $\overset{\circ}{\mathbb{M}}$ the operators for $h_{\alpha\beta}=0$ and by $\overset{\circ}{\mathbb{G}}_{\sigma}$, $\overset{\circ}{\mathbb{K}}$ and $\overset{\circ}{\mathbb{M}}$ their linear order $\sim h_{\alpha\beta}$. The zeroth and first order terms of the expansion of the electric scattering Green tensor in surface curvature can be expressed in compact notation as

$$\Gamma = \begin{pmatrix} 0 & (EE) \\ \mathbb{G}_{0} \\ 0 & (EH) \end{pmatrix} \mathbb{O} \begin{pmatrix} 0 & (EE) \\ \mathbb{M} \\ 0 & (EH) \end{pmatrix} \\
\Gamma = \begin{pmatrix} 1 & (EE) \\ \mathbb{G}_{0} \\ 0 & (EH) \\ \mathbb{G}_{0} \end{pmatrix} \mathbb{O} \begin{pmatrix} 0 & (EE) \\ \mathbb{M} \\ 0 & (EH) \\ \mathbb{M} \end{pmatrix} + \begin{pmatrix} 0 & (EE) \\ \mathbb{G}_{0} \\ 0 & (EH) \\ \mathbb{G}_{0} \end{pmatrix} \mathbb{O} \begin{pmatrix} 1 & (EE) \\ \mathbb{M} \\ 1 & (EH) \\ \mathbb{M} \end{pmatrix} + \begin{pmatrix} 0 & (EE) \\ \mathbb{G}_{0} \\ 0 & (EH) \\ \mathbb{M} \end{pmatrix} \mathbb{O} \mathbb{KO} \begin{pmatrix} 0 & (EE) \\ \mathbb{M} \\ 0 & (EH) \\ \mathbb{M} \end{pmatrix}$$
(19)

with

$$\mathbb{O} = \left(\mathbb{1} - \mathbb{K}\right)^{-1} = \begin{pmatrix}
\mathbb{R} & \mathbb{RK} \\
{}_{0}(HE) \\
\mathbb{K} & \mathbb{R}
\end{pmatrix}$$

$$\mathbb{R} = \left(\mathbb{1} - \mathbb{K} & \mathbb{K}\right)^{-1}$$

$$(20)$$

where we used that $\mathbb{K} = 0$, $\mathbb{K} = 0$. We use

the Fourier representation of \mathbb{G}_{σ} and carry out analytically the integrations over the wave vector along the $\hat{\mathbf{z}}$ direction and the angle of the in-plane $\hat{\mathbf{x}}$ - $\hat{\mathbf{y}}$ wave vector. This yields to zeroth order the diagonal tensor $4\pi\kappa \, \mathbb{F} = d^{-3} \, \mathrm{diag}(\beta_1^{(0)}, \beta_1^{(0)}, \beta_2^{(0)})$ with

$$\beta_{1}^{(0)} = \int_{0}^{\infty} \bar{k} d\bar{k} \frac{e^{-2s_{0}} \left(2\bar{\kappa}^{4} \mu_{0}^{2} \epsilon_{0}^{2} s_{1} (\mu_{0} \epsilon_{1} - \mu_{1} \epsilon_{0}) + 3\bar{\kappa}^{2} \bar{k}^{2} \mu_{0} \epsilon_{0} s_{1} (\mu_{0} \epsilon_{1} - \mu_{1} \epsilon_{0}) + \bar{k}^{4} \left(\epsilon_{1} \left(\mu_{1} s_{0} + \mu_{0} s_{1} \right) - \epsilon_{0} \left(\mu_{0} s_{0} + \mu_{1} s_{1} \right) \right) \right)}{2\epsilon_{0} s_{0}^{2} \left(\mu_{1} \epsilon_{0} \left(s_{0} s_{1} + 2\tilde{\kappa}^{2} \mu_{0} \epsilon_{1} \right) + \mu_{0} \epsilon_{1} s_{0} s_{1} + \bar{k}^{2} (\mu_{0} \epsilon_{0} + \mu_{1} \epsilon_{1}) \right) \right)}$$

$$\beta_{2}^{(0)} = \int_{0}^{\infty} \bar{k} d\bar{k} \frac{e^{-2s_{0}} \left(\bar{k}^{4} \left(\mu_{1} \epsilon_{1} - \mu_{0} \epsilon_{0} \right) + \bar{k}^{2} s_{0} s_{1} \left(\mu_{0} \epsilon_{1} - \mu_{1} \epsilon_{0} \right) \right)}{\epsilon_{0} s_{0} \left(\bar{k}^{2} \left(\mu_{0} \epsilon_{0} + \mu_{1} \epsilon_{1} \right) + \mu_{1} \epsilon_{0} \left(s_{0} s_{1} + 2\tilde{\kappa}^{2} \mu_{0} \epsilon_{1} \right) + \mu_{0} s_{0} s_{1} \epsilon_{1} \right)}$$

where $s_{\sigma} = \sqrt{\bar{k}^2 + \mu_{\sigma} \epsilon_{\sigma} \bar{\kappa}^2}$. Here we have introduced the rescaled quantities $\bar{k} = dk$, $\bar{\kappa} = d\kappa$ so that $\beta_1^{(0)}$ and $\beta_2^{(0)}$ are dimensionless. The next order, which is linear in curvature, assumes the form

$$4\pi\kappa \stackrel{1}{\mathbb{\Gamma}}^{(EE)} = \frac{1}{d^2} \begin{pmatrix} \left(\beta_1^{(2)} + \frac{1}{2}\beta_3^{(2)}\right) h_{11} + \left(\beta_1^{(2)} - \frac{1}{2}\beta_3^{(2)}\right) h_{22} & \beta_3^{(2)} h_{12} & 0 \\ \beta_3^{(2)} h_{12} & \left(\beta_1^{(2)} - \frac{1}{2}\beta_3^{(2)}\right) h_{11} + \left(\beta_1^{(2)} + \frac{1}{2}\beta_3^{(2)}\right) h_{22} & 0 \\ 0 & 0 & \beta_2^{(2)} \left(h_{11} + h_{22}\right) . \end{pmatrix}$$
(22)

Here the β coefficients are given by k-integrals similar to those in Eq. (21) but there are expressions are too long to be shown here. Instead there are provided in a supplementary Mathematica notebook. When the expressions ${}^{0}(EE)$ and 1 are substituted into Eq. (2) of the main text, one obtains the CP potential in Eq. (4) of the main text.

- M. Bordag, G. L. Klimchitskaya, U. Mohideen and V. M. Mostepanenko, Advances in the Casimir Effect (Oxford University Press, 2009).
- [2] L. Bergstrom, Hamaker constants of inorganic materials. Advances in Colloid and Interface Science 70, 125-169 (1997).
- [3] D. B. Hough and L. R. White, The calculation of Hamaker constants from Liftshitz theory with applications to wet-

- ting phenomena. Advances in Colloid and Interface Science 14, 3-41 (1980).
- [4] R.S. Decca, D. Lopez, E. Fischbach, G.L. Klimchitskaya, D.E. Krause and V.M. Mostepanenko, Novel constraints on light elementary particles and extradimensional physics from the Casimir effect, Eur. Phys. J. C 51, 963 (2007).
- [5] V. A. Parsegian, Van der Waals Forces: A Handbook for Biologists, Chemists, Engineers, and Physicists (Cambridge University Press: New York, NY, USA, 2006).
- [6] V. N. Marachevsky, Casimir Effect and Quantum Field

- Theory in dielectrics, Theor. Math. Phys. 131, 468 (2002).
- [7] S.Y. Buhmann H.T. Dung, D.G. Welsch, The van der Waals energy of atomic systems near absorbing and dispersing bodies, J. Opt. B Quantum Semiclass. Opt. 6, S127 (2004). conductors with edges and tips, Proc. Natl. Acad. Sci.
 - conductors with edges and tips, Proc. Natl. Acad. Sci USA 108, 6867 (2011).
- [8] G. Bimonte and T. Emig, Casimir and Casimir-Polder interactions for magneto-dielectric materials: Surface scattering expansion, Phys. Rev. A 108, 052807 (2023).

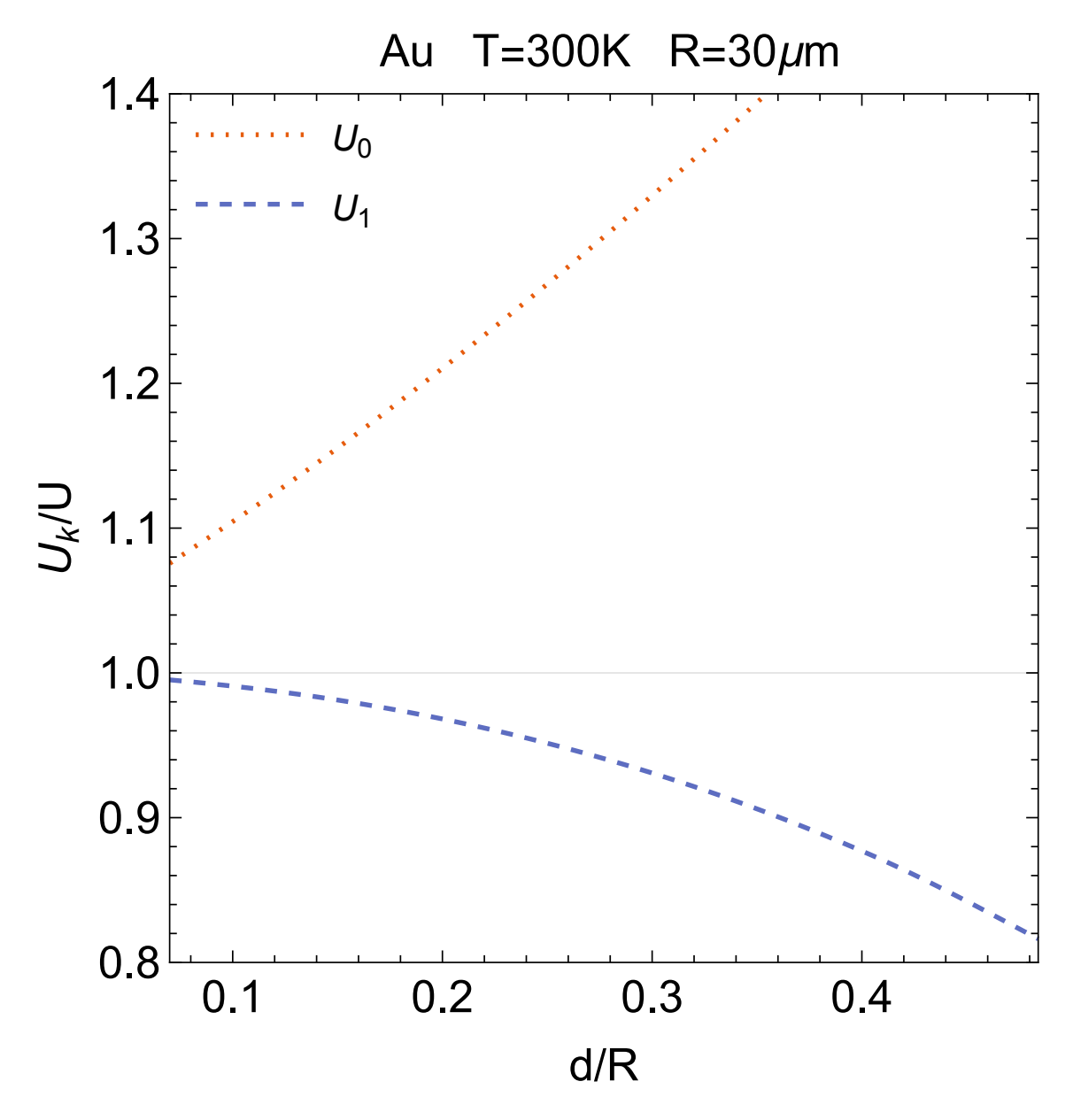


FIG. 5. Ratio of the curvature expansion of the CP potential U_k up to the k-th power of d/R to the exact potential U_{sphere} for an Au sphere of radius $R=30\mu\text{m}$ at T=300K versus the normalized distance d/R.